Surface & Coatings Technology 344 (2018) 702–709

Contents lists available at ScienceDirect

Surface & Coatings Technology

journal homepage: www.elsevier.com/locate/surfcoat

Fabrication and corrosion property of conversion films on magnesium alloy from deep eutectic solvent

Jialei Zhang[a,b], Changdong Gu[a,b,*], Wei Yan[a,b], Jiangping Tu[a,b], Xiangdong Ding[c,**]

[a] School of Materials Science and Engineering, State Key Laboratory of Silicon Materials, Zhejiang University, Hangzhou 310027, People's Republic of China
[b] Key Laboratory of Advanced Materials and Applications for Batteries of Zhejiang Province, Hangzhou 310027, People's Republic of China
[c] State Key Laboratory for Mechanical Behavior of Materials, Xi'an Jiaotong University, Xi'an 710049, People's Republic of China

ARTICLE INFO

Keywords:
Mg alloy
Conversion film
Anodic treatment
Deep eutectic solvent
Corrosion resistance

ABSTRACT

A facile anodic treatment for magnesium alloy was proposed in a choline chloride-ethylene glycol based deep eutectic solvent (DES). Conversion films with interconnected porous networks and jagged nanorod arrays can be formed, which depends on the applied anodic current density. Crystallographic orientation of the substrate is accordingly changed. The conversion films are mainly composed of $MgCO_3$ which results from the interaction between the Mg alloy and the released species from the decomposition of DES. A higher anodic current density produces a better corrosion resistant conversion film. Superhydrophobic and slippery surfaces can be achieved on the as-prepared conversion films to further improve the corrosion resistance.

1. Introduction

Magnesium and its alloys have been extensively used in the fields of automotive, aerospace, electronics and biomedicine owing to their attractive properties including high specific strength, considerable ductility, improved machinability, good castability, excellent biocompatibility and available recyclability [1–4]. However, a fatal flaw of Mg alloys is the poor corrosion resistance caused by the inherently high activity of Mg. Natural corrosion products such as oxides, hydroxides and carbonates on Mg alloys cannot provide a uniform and large-area passive film [5]. Artificial conversion coatings seem to be one of the effective ways to enhance the corrosion resistance [6–8]. In recent years, various conversion coatings on Mg alloys have been developed with advantages of facile procedure, tunable texture and high adhesion to substrate, e.g. phytic acid [9], chromate [10], phosphate [11–13], stannate [14,15], vanadate [16,17], permanganate [18], fluoride [2], and hydrotalcite coatings [19–21]. However, most of these coatings or films are synthesized from conventional aqueous reaction media, which results in hydrogen evolution and uncontrollable preparation [22]. In comparison with the widely studied water-based system, non-aqueous solvents show prospective alternatives for preparing superior coatings or films on Mg alloys [23].

Ionic liquids are room-temperature molten salts composed entirely of cations and anions, which are regarded as a new type of solvent except aqueous and organic solvents. Active metals such as magnesium and lithium remain stable for a long time without being corroded in specific ionic liquids owing to no free H^+ or other metal cations, which provides favorable conditions for the control of film formation on active metals [24–29]. M. Forsyth's group proposed a surface treatment of the AZ31 Mg alloy in biocompatible phosphate-based ionic liquids to mitigate its degradation in human body [24]. They evaluated the cytotoxicity and corrosion resistance of the ionic liquid films and found the corrosion resistance was depended on the treatment time. When a potential bias of −200 mV was applied on the ZE41 Mg alloy during exposure to the ionic liquid of trihexyl(tetradecyl)phosphonium diphenylphosphate, a more uniform ionic liquid film would be formed compared with the one obtained at open circuit potential [29].

Choline chloride (ChCl) based deep eutectic solvents (DESs) are a new class of ionic liquids or ionic liquid analogues sharing most of their remarkable qualities while possessing other advantages such as easy synthesis, low cost facile application and so on [30]. They have been applied for coating electrodeposition, surface electropolishing, nanomaterial synthesis, and biotransformation [31,32]. Our group has reported that the ChCl-urea based DES would decompose under thermal conditions to generate ammonia/amide and carbonate in the presence of a little water [33]. Upon heating, the ChCl-urea mixture could react with the AZ31B Mg alloy to form a promising anti-corrosion conversion film [23]. It was also demonstrated that the trivalent chromium conversion coating with self-healing effect could be fabricated by utilizing the interaction between the ChCl-ethylene glycol-$CrCl_3$ solution and the

* Correspondence to: C. Gu, School of Materials Science and Engineering, State Key Laboratory of Silicon Materials, Zhejiang University, Hangzhou 310027, People's Republic of China.
** Corresponding author.
E-mail addresses: cdgu@zju.edu.cn (C. Gu), dingxd@mail.xjtu.edu.cn (X. Ding).

https://doi.org/10.1016/j.surfcoat.2018.04.004
Received 1 February 2018; Received in revised form 22 March 2018; Accepted 2 April 2018
Available online 03 April 2018
0257-8972/

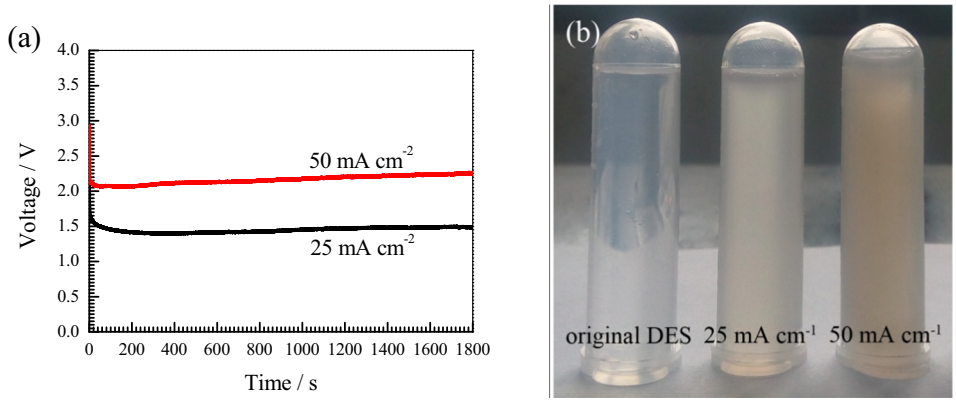

Fig. 1. (a) Chronopotentiometric curves at different current densities during the anodic treatments. (b) Visual inspections of the original DES and the electrolytes after anodic treatments at different current densities.

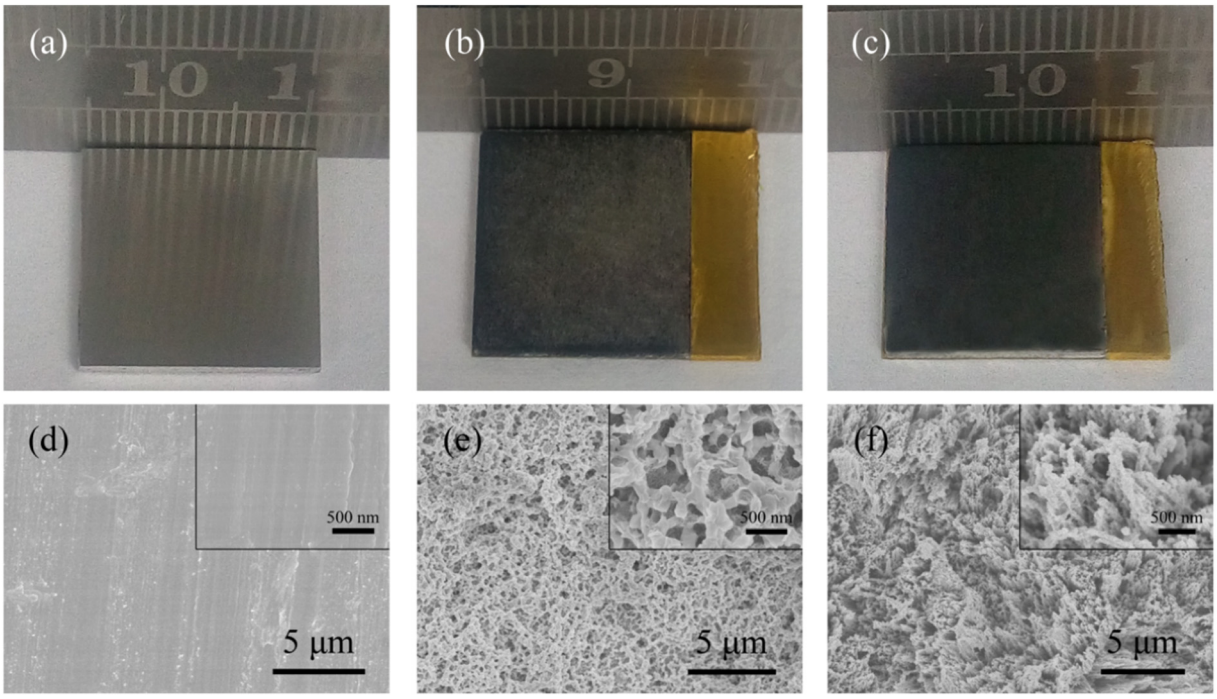

Fig. 2. Optical photographs and SEM images of the bare and anodic treated Mg alloy substrates. (a, d) bare Mg alloy, (b, e) CF-25 and (c, f) CF-50. Insets of the SEM images show the magnified views.

Mg alloy substrate under an ultrasonic condition [34]. Therefore, it would be promising that more effective coatings or films might be produced on Mg alloys by adopting different external fields at the ionic liquid/substrate interface. DESs would decompose at both electrodes over long periods of electrolysis to form chlorinated products and organic compounds via Hoffman elimination [35]. The decomposition of DESs would produce anions and cations which have different affinity for absorption on the Mg alloy surface. Therefore, conversion films could form by interactions between the decomposition products and the Mg alloy [23].

An electric field was applied to stimulate the decomposition of DES and facilitate the reaction of DES/Mg alloy interface in the present work. Interestingly, conversion films with various nanostructures were formed on the Mg alloy substrates by the proposed anodic treatment in the DES. Superhydrophobic surface (SHS) and slippery lubricant-infused porous surface (SLIPS) were further endowed to the conversion films under the inspiration of natural *Nepenthes* pitcher plants. The composition, structure and corrosion behavior of the conversion films were investigated. Moreover, a possible film formation mechanism was proposed. This work is anticipated to stimulate the practical application of DESs in the surface treatment of Mg alloys for corrosion protections.

2. Experimental

2.1. Preparation of conversion films and the following surface modifications

Choline chloride [$HOC_2H_4N(CH_3)_3^+$ Cl^-] (analytical reagent, purity ≥ 98.0%) and ethylene glycol [$(CH_2OH)_2$] (analytical reagent, purity ≥ 99.0%) were mixed in a 1:2 mol ratio without further purification and subsequently stirred at 80 °C until a homogeneous DES formed. AZ31B Mg alloy substrates (45 mm × 17 mm × 1 mm) were previously abraded by SiC papers up to 1000 grit, and then ultrasonically washed in an acetone (analytical reagent, purity ~99.7%) bath. Each pretreated substrate was sealed by polyimide tapes leaving a single side of 15 mm × 17 mm. A facile anodic treatment was performed in a chronopotentiometry mode using a two-electrode electrochemical cell (CHI660e, Chenhua Instruments Inc., China). The anodic voltage was enabled through tuning current density. An unsealed Mg

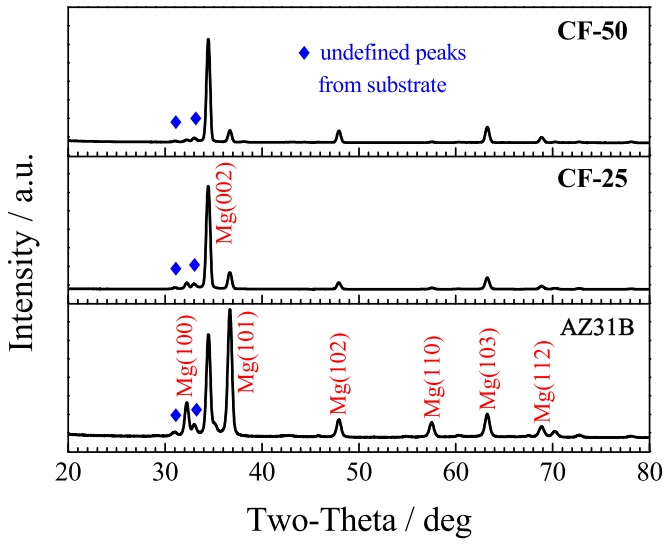

Fig. 3. XRD patterns of the bare AZ31B Mg alloy substrate and the anodic treated CF-25 and CF-50. No film or reaction product is identified in these specimens except a hexagonal Mg phase (JCPDS 35-0821) from the Mg alloy. But the surface crystallographic orientation of the substrate is changed after the anodic treatment.

alloy was used as the counter electrode (cathode) and the sealed Mg alloy (15 mm × 17 mm) was used as the working electrode (anode). The DES was served as electrolyte, which was stirred at about 800 rpm and kept at 85 ± 3 °C. Conversion films were formed on the Mg alloy substrates after 30 min at the current density of 25 and 50 mA cm^{-2}. The corresponding specimens are hereafter denoted as CF-25 and CF-50, respectively. Finally, the specimens were sequentially rinsed by methanol (analytical reagent, purity ~99.7%) and de-ionized water, and then dried in flowing nitrogen.

SHSs were obtained by immersing the as-prepared CF-25 and CF-50 into a solution of ethanol (analytical reagent, purity ~99.7%) containing 0.5 wt% 1H,1H,2H,2H-perfluorooctyltriethoxysilane (PTES, Amethyst®, purity ~97%) for 2 h at room temperature, and followed by drying them in an oven for 1 h at 120 °C. The above SHSs are denoted as SHS-25 and SHS-50, respectively. Furthermore, excess lubricant, perfluoropolyether (Fomblin® YR-1800) liquid, was dropped onto the SHS-25 and SHS-50 to obtain SLIPS-25 and SLIPS-50, respectively. After completely spreading and permeating the whole SHSs, the specimens were vertically hung at laboratory environment for 3 days to drain off the excess liquid. It was measured that the lubricant sealed in each specimen was ~3.5 mg cm^{-2}.

2.2. Structural characterization and wettability

A field emission scanning electron microscope (FE-SEM, Hitachi SU-70) was employed to observe the surface morphology. X-ray diffraction (XRD, XPert Pro-MPD with CuKα radiation, λ = 0.15406 nm) and transmission electron microscopy (TEM, FEI Tecnai G2F20 S-Twin) were applied to analyze the crystalline structure. Debris was physically scraped from the conversion films for TEM observations. Surface chemical state was detected by X-ray photoelectron spectroscopy (XPS, AXIS UTLTRADLD) using monochromatic AlK_α radiation with E = 1486.6 eV after Ar ion sputtering. The XPS core-level spectra were referred to C 1 s peak at 284.6 eV and analyzed through peak fitting (XPSPEAK Version 4.1). Fourier transform infrared (FT-IR, Nicolet iS50) spectra were collected using KBr pellets (conversion films were physically scraped from the substrate and pressed into pellets).

Water contact angle (CA) and sliding angle (SA) were determined by a contact angle meter (SL200B, Solon Tech.) based on a sessile drop measuring method with a water droplet volume of 4 μl or 8 μl. CA hysteresis of the SLIPSs was also revealed by the advancing (θ_A) and receding (θ_R) CAs measured as the substrates were tilted by ~10°.

2.3. Electrochemical measurements

Corrosion resistance was evaluated by potentiodynamic polarization measurements and immersion experiments in a 3.5 wt% NaCl (analytical reagent, purity ~99.5%) aqueous solution at room temperature. Polarization curves were recorded by a three-electrode cell (Chenhua Instruments Inc., China) with Pt as counter electrode and Ag/AgCl (saturated KCl) as reference electrode at a scan rate of 1 mV s^{-1}. The working electrode was the specimen covered by polyimide tapes leaving an exposed area of ~1 cm^2, which was exposed in the solution for about 20 min to stabilize the open circuit potential before each test. Corrosion potential (E_{corr}) and corrosion current density (i_{corr}) were derived (Tafel extrapolation) from the polarization curves. The covered specimens were also immersed in the 3.5 wt% NaCl solution, after which the morphologies were observed. All the experiments and

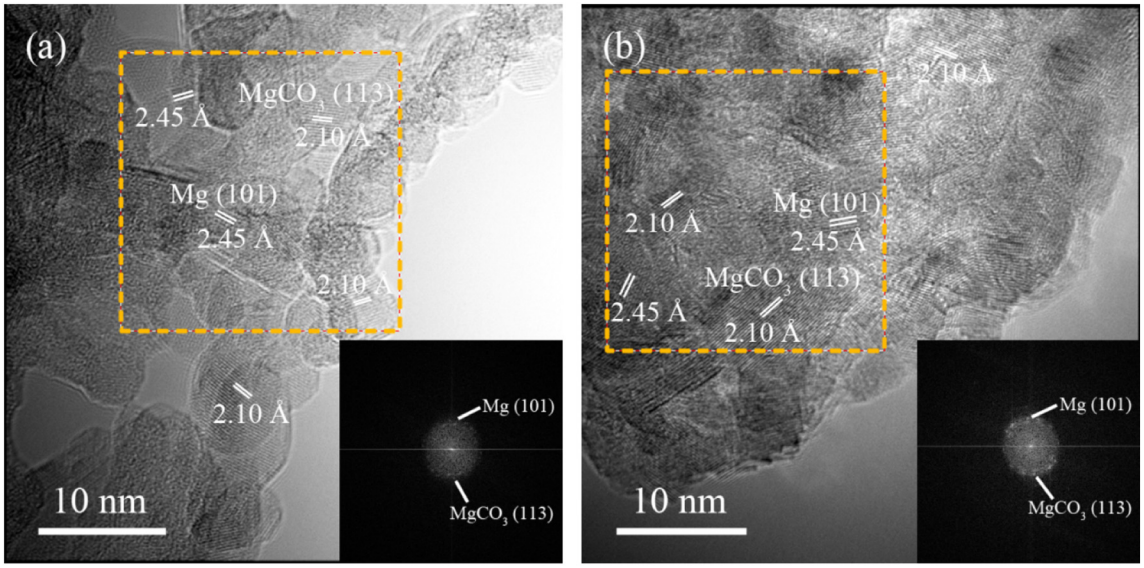

Fig. 4. HR-TEM images of the debris scraped from the CF-25 (a) and CF-50 (b). Lattice fringes with crystal plane spacing of 2.45 Å and 2.10 Å are assigned to Mg (101) planes and $MgCO_3$ (113) planes, respectively. FFT images corresponding to the frames are given in the insets.

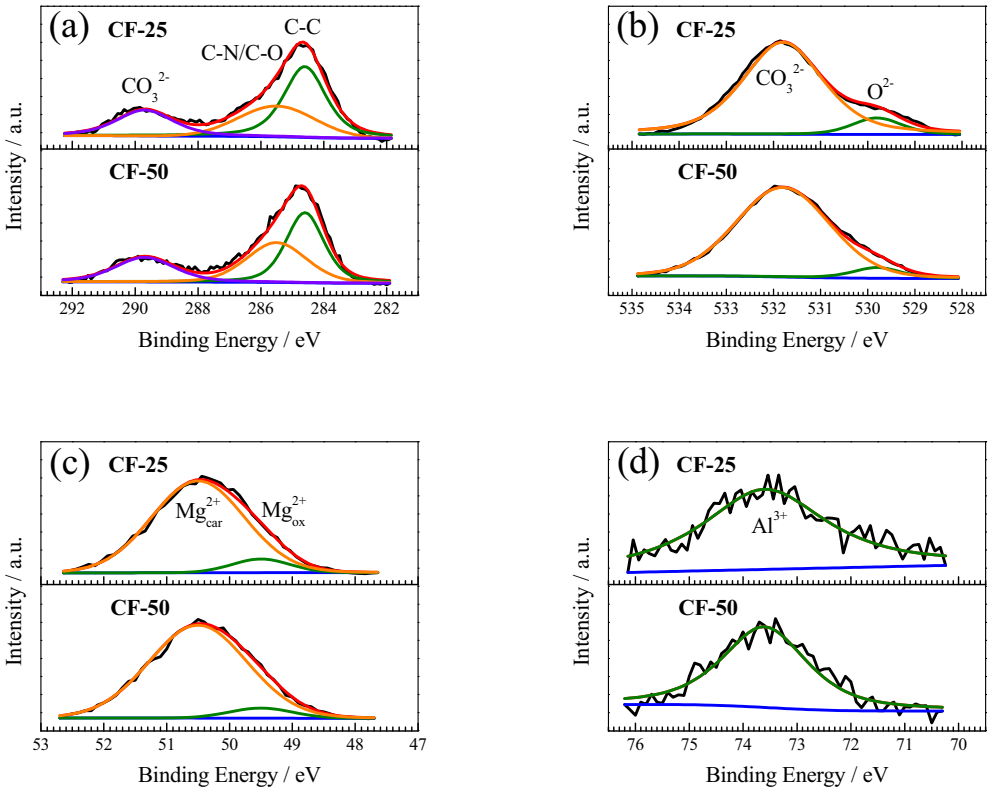

Fig. 5. XPS core-level spectra of the anodic treated CF-25 and CF-50. (a) C 1 s, (b) O 1 s, (c) Mg 2p and (d) Al 2p.

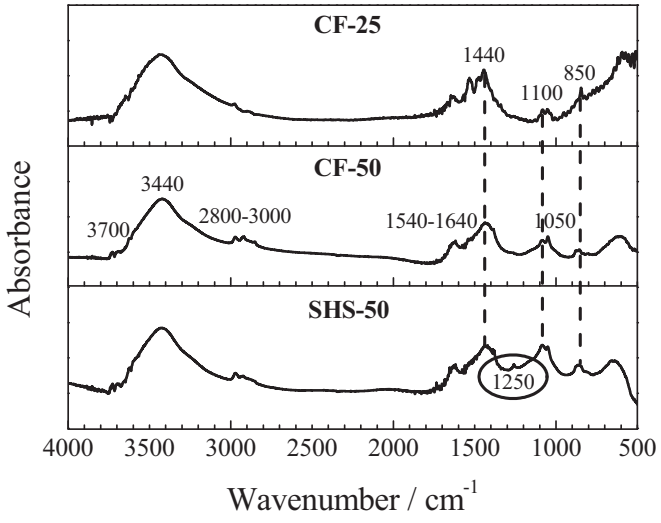

Fig. 6. FT-IR spectra of the powders scraped from the CF-25, CF-50 and SHS-50.

measurements were repeated at least three times to ensure the reproducibility.

3. Results and discussion

ChCl-ethylene glycol based DES is an air-stable ionic liquid that is inert to common metals like Fe, Al, Ni etc. [36] We also found that pure ChCl-ethylene glycol solution was almost unable to react with the AZ31B Mg alloy even at a high temperature of ~85 °C. Therefore an assistant electric field was further introduced to facilitate the interface reactions between the DES and Mg alloy for producing a novel film. Fig. 1a and b show the chronopotentiometric curves at different current densities and the visual changes of the DES electrolytes after the anodic treatments, respectively. The voltage is detected at the working electrode once the current is set, as presented in Fig. 1a. At the current densities of 25 and 50 mA cm^{-1}, the voltages are stabilized at about 1.5 and 2.0 V (vs. AZ31B), respectively. Both the curves have a sharp decline in the first several seconds and a gentle increase in the subsequent process. The initial voltage decline probably results from the instrument stabilization. Conversion films are likely to be formed and increase the polarization at the DES/electrode interface, which leads to the following voltage increase. Mg alloy substrate is gradually dissolved into the DES due to the anodic voltage. As a result, the DES electrolyte turns from colorless clear (b0) to gray or dark muddy (b1 and b2). The decomposition products at anode include Cl_3^- species and make the solution turn out to be brown [35]. This process is analogous to the reported electropolishing of stainless steels in the DES [37]. In addition, bubbles were generated at the electrodes during the long-time electrochemical treatment at such a high overvoltage [38]. It indicated a severe decomposition of the DES as polarization occurred with the formation of conversion films. We also found film-like products formed on the opposite electrode (i.e. the cathodic Mg alloy) during the experiment, which will be investigated in further study.

Fig. 2 displays the optical photographs and SEM images of the bare and anodic treated Mg alloy substrates. The mechanically polished Mg alloy substrate possesses a smooth and bright surface with metallic luster. Repeatable experiments showed that the CF-50 was visually more uniform than the CF-25, as presented in Fig. 2b and c. After anodic treatments, the substrates are uniformly covered by dark conversion films and exhibit rough surfaces. Three-dimensional porous network-like structures are interconnected on the CF-25 surface, as shown in Fig. 2e. Numerous small openings with the aperture size of 100–500 nm are evenly distributed in the networks. The frameworks of the network are smooth and coherent. By contrast, three-dimensional porous arrays are observed on the CF-50 surface, as shown in Fig. 2f. The jagged arrays are constituted by closely arranged nanorods with a diameter of ~100 nm. The surfaces of the nanorods are rough and

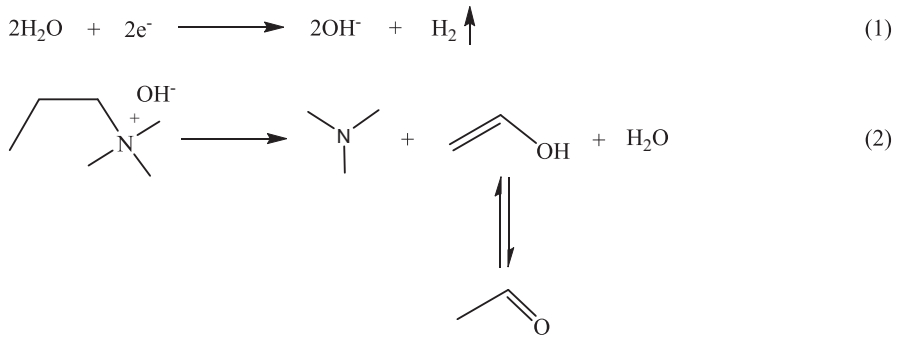

Scheme 1. Possible chemical reactions at the cathode during the anodic treatment in the DES. (1) H_2 evolution in electrolysis of H_2O. (2) Hoffman elimination of choline hydroxides proposed by the reference [35].

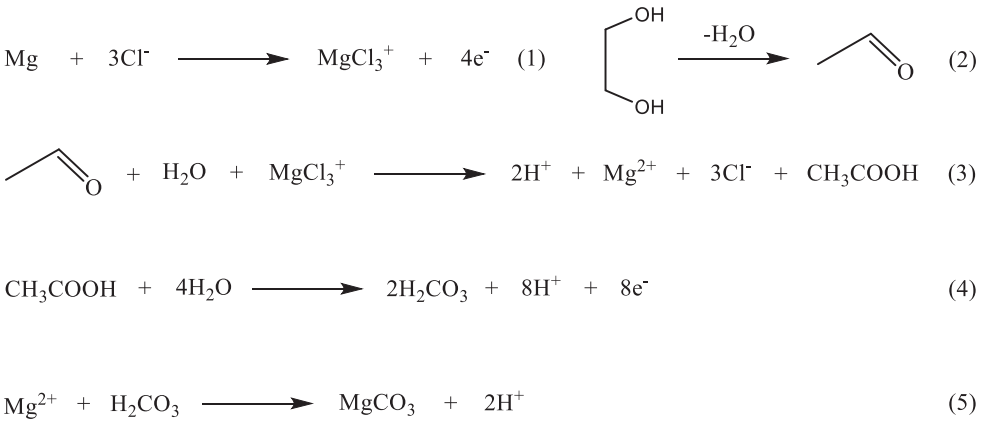

Scheme 2. Possible chemical reactions at the anode in the DES. (1) Dissolution of Mg. (2) Dehydration of ethylene glycol proposed by the reference [35]. (3) Oxidation of acetaldehyde by Cl_3^- species. (4) Electrolysis of acetic acid. (5) Formation of $MgCO_3$ on the Mg alloy.

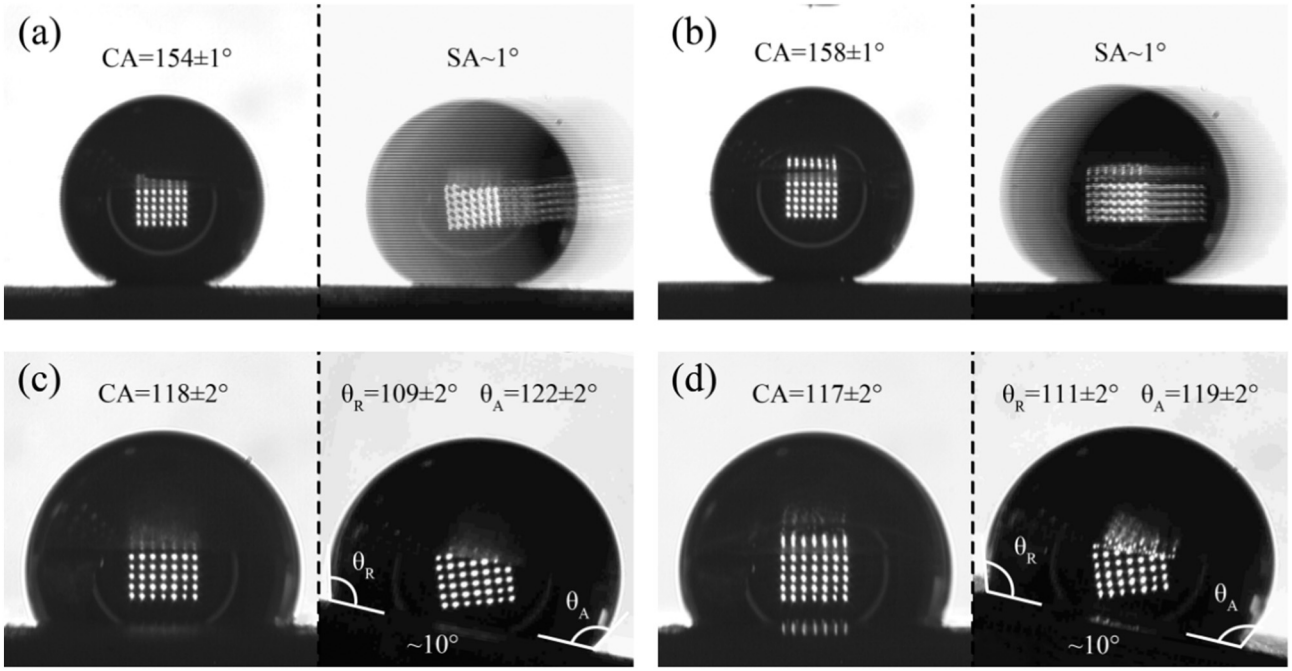

Fig. 7. 4 μl of water droplets on the SHS-25 (a), SHS-50 (b) and 8 μl of water droplets on the SLIPS-25 (c), SLIPS-50 (d). Static water CA values are measured from the left photographs of each picture. Water SAs, advancing (θ_A) and receding (θ_R) CAs are determined by the right snapshots. Water droplets quickly roll off the SHSs with SA of ~1°, but slowly slide off the SLIPSs as the substrates are tilted by ~10°.

structured. Therefore, the higher anodic current density results in a significantly rougher surface of the conversion film.

XRD patterns of the bare and anodic treated AZ31B Mg alloy substrates are presented in Fig. 3. There is no peak corresponding to any films or reaction products except the identified hexagonal Mg phase (JCPDS 35-0821) from the Mg alloy substrate, which should be

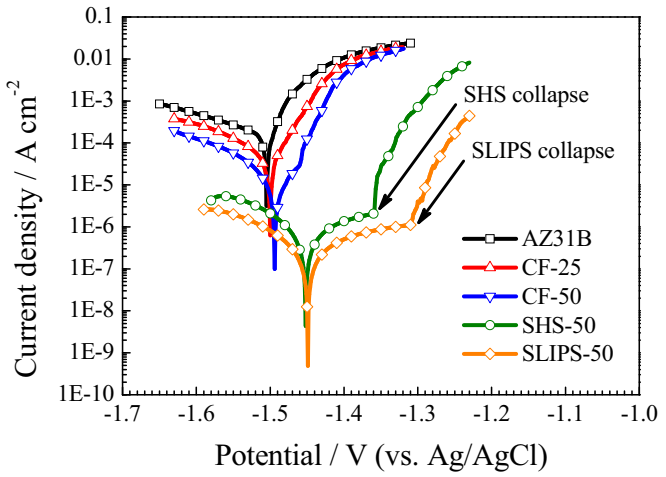

Fig. 8. Polarization curves of the bare AZ31B, CF-25, CF-50, SHS-50 and SLIPS-50 in a 3.5 wt% NaCl aqueous solution at room temperature. The scan rate is 1 mV s^{-1} (vs. Ag/AgCl).

Table 1
Corrosion parameters of the bare AZ31B, CF-25, CF-50, SHS-50 and SLIPS-50 summarized from the polarization curves. The potentials are referenced to the Ag/AgCl electrode.

Sample	AZ31B	CF-25	CF-50	SHS-50	SLIPS-50
E_{corr} (mV)	−151	−150	−149	−145	−145
i_{corr} (μA cm^{-2})	988	66.5	27.7	0.711	0.263

attributed to the thin and very small quantity of the film. Therefore the following TEM detections are necessary. Interestingly, a significant weakened peak intensity ratio of (101) to (002) planes of hexagonal Mg is found in the conversion films compared to that in the AZ31B Mg alloy substrate. For instance, the intensity ratio of (101) over (002) planes, I(101)/I(002), is about 1.24, 0.17 and 0.13 for the AZ31B, CF-25 and CF-50, respectively. Besides, the intensity ratio of (100) over (002) planes, I(100)/I(002), for the conversion films is also decreased. It indicates that the (101) and (100) planes of Mg are priority to be dissolved. Moreover, the higher voltage induced by higher anodic current density promotes the preferential dissolution of the substrate. Consequently, the current density-dependent structure and morphology of the conversion film are closely related to the selective dissolution of the substrate and the complicated film growth process.

TEM observations are performed to further explore the structure and composition of the as-prepared conversion films. Typical high-resolution TEM (HR-TEM) images of the debris scraped from the conversion films are given in Fig. 4. The CF-25 and CF-50 exhibit similar crystal structures and both of them are composed of nanocrystals with an average grain size of ~10 nm. Lattice fringes with crystal plane spacing of 2.45 Å are corresponding to Mg (101) planes from the substrate and those with crystal plane spacing of 2.10 Å are assigned to $MgCO_3$ (113) planes (JCPDS 08-0479). These results are also confirmed by fast Fourier transform (FFT) analyses, as shown in the insets. On account of the similar plane spacing of MgO (200) planes (JCPDS 78-0430) to that of $MgCO_3$ (113) planes, it is hardly to confirm the existence of MgO in the conversion films. Hence, XPS was adopted to reveal the surface composition of the conversion films.

Fig. 5 exhibits the C 1 s, O 1 s, Mg 2p and Al 2p core-level XPS spectra of the anodic treated CF-25 and CF-50. All the peaks are referred to C 1 s peak at the binding energy of 284.6 eV corresponding to C—C species. Similar fitting results are obtained for the CF-25 and CF-50, which indicates the same composition of the conversion films prepared at different anodic current densities. For the C 1 s spectra, the other two peaks are assigned to the C—N or C—O structure at 285.7 eV and the CO_3^{2-} components at 289.7 eV, respectively [27,39]. They can be recognized as the impurities from the ChCl-based DES and the $MgCO_3$ from the conversion film, respectively. The O 1 s spectra are well fitted by two peaks at 529.8 eV for O^{2-} in oxides and at 531.8 eV for CO_3^{2-} in carbonates [19]. The sole peak of Mg 2p also contains Mg^{2+} in its oxides (49.5 eV) and carbonates (50.5 eV) [40]. The peak intensity of oxides is much lower than that of carbonates either in the O 1 s or Mg 2p spectra, which means $MgCO_3$ is the mainly component of the conversion film. Moreover, Mg hydroxides have not been formed in the products from the applied non-aqueous DES, which is in accordance with the previous works [23,34]. It is ascribed to the very low content of water in the DES and the trace amount of OH^- generated at anode [35]. The trace amount of Al exists as Al^{3+}, probably Al_2O_3, in the conversion films. Till now, it is rational to conclude that the conversion films are mainly composed of $MgCO_3$ with little MgO.

Since organic impurities would be brought out from the DES, the FT-IR spectra are detected and displayed in Fig. 6 to identify functional groups in the conversion films. The characteristic absorption peaks at about 1440 (ν_3), 1100 (ν_1) and 850 (ν_2) cm^{-1} confirm the CO_3^{2-} group [41–43]. Choline chloride shows the FT-IR bands between 2800 and 3000 cm^{-1} corresponding to the C—H stretching of the –CH_3 and —CH_2— groups, and the band at ~1050 cm^{-1} due to the stretching vibration of C—C—O groups [44]. The significant absorption peaks in this range (around 2890 cm^{-1}) have been assigned to the symmetric-antisymmetric stretches of NH_4^+ ν_1–ν_3 in combination with water ν_1–ν_3 [45]. Accordingly, the absorbance band at ~3440 cm^{-1} corresponds to adsorbed water, and the bands between 1540 and 1640 cm^{-1} are attributed to the ν_2 (H—O—H) deformation in water and ν_2 (NH_4^+) stretching vibration in ammonium [45]. It suggests that amine or ammonium is generated and incorporated in the conversion films along with the choline chloride molecules. These organic impurities can be hardly washed up by water or methanol. The very weak bands at ~3700 cm^{-1} might be assigned to the lattice vibration of $Mg(OH)_2$ which results from the trace amount of MgO reacting with water [41,45]. An additional absorption peak at 1251 cm^{-1} is observed for the SHS-50, which represents the —CF_2— group in the molecular structure of PTES [46]. Other peaks such as 1320 cm^{-1} for —CF_3 and 1070 cm^{-1} for —Si—O—Si— are not significant in intensity probably due to their low quantity in the molecular structure of PTES. Therefore, the component of $MgCO_3$ is confirmed, and the impurities of ammonium and choline chloride are detected in the conversion films by FT-IR spectra.

According to the reference [35], choline base (choline hydroxide) is easily formed at the cathode where OH^- concentration is high because of the reduction of trace water without other metal cations in the DES (Eq. (1) of Scheme 1). In this case, Hoffman elimination of choline hydroxides occurs (Eq. (2) of Scheme 1). Herein, the product of H_2O in (2) would be further electrolyzed through (1). This progress seems to be a rational explanation for the observed bubble evolution at cathode. As for anode, the chemical reactions should be much more complicated. Herein, we proposed a possible approach for the anodic reactions. On the one hand, the Mg alloy is gradually dissolved into the DES, which could be described as Eq. (1) of Scheme 2. It should be noted that Cl_3^- species are liable to remain in the DES instead of Cl_2 gas and react as an oxidant [35]. Meanwhile, the dehydration of ethylene glycol would produce the acetaldehyde (Eq. (2) of Scheme 2), which should be the primary source of acetaldehyde except the product of Hoffman elimination [35]. On the other hand, the Cl_3^- species with strong oxidation could easily oxidize acetaldehyde to acetic acid which is further electrolyzed to generate H_2CO_3 around the anode (Eqs. (3) and (4) of Scheme 2). $MgCO_3$ could be deposited on the Mg alloy substrate (Eq. (5) of Scheme 2). As the predominant reaction (Eq. (1) of Scheme 2), the dissolution of Mg maintains during the anodic treatment, thus the newly formed $MgCO_3$ based conversion film cannot grow very thick. It is a dynamic equilibrium between the substrate dissolution and the film formation. Further investigations on film formation mechanism would

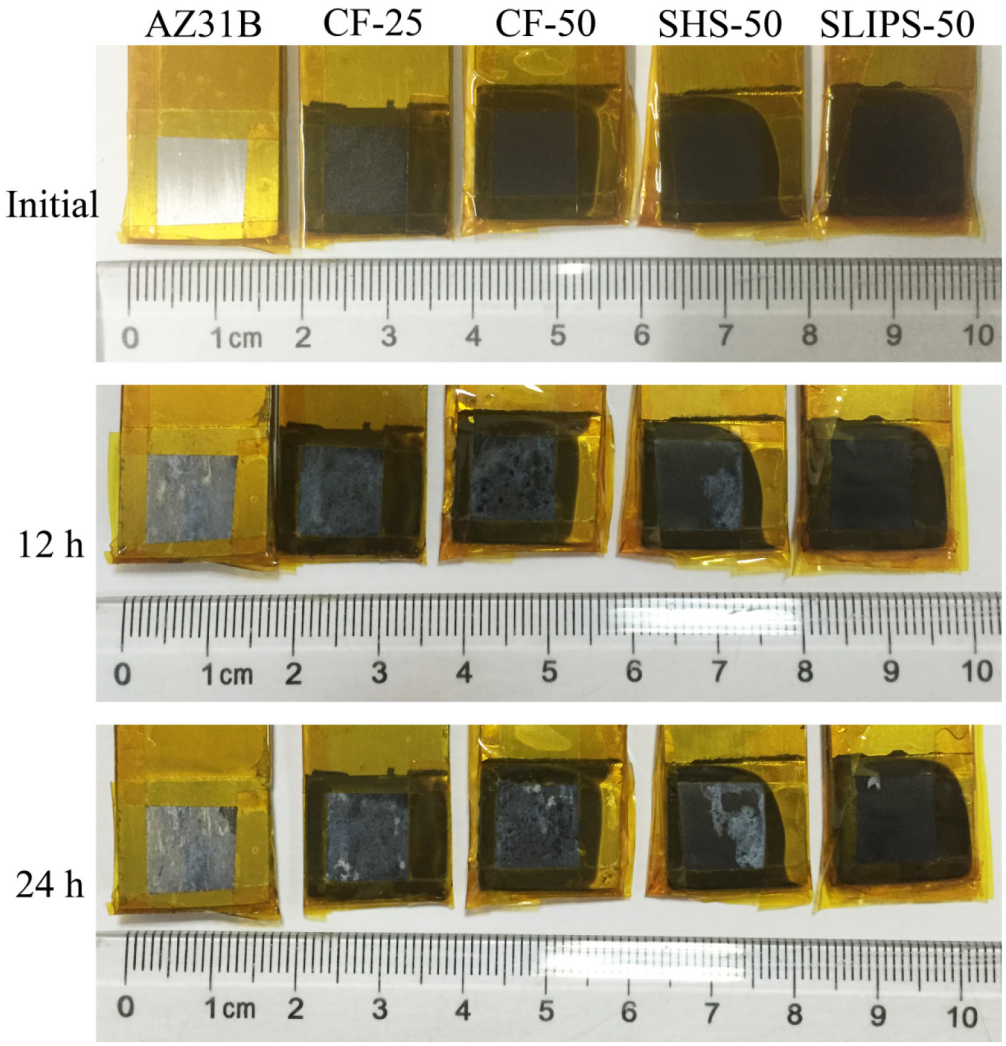

Fig. 9. Optical photographs of the bare AZ31B, CF-25, CF-50, SHS-50 and SLIPS-50 after immersing in the 3.5 wt% NaCl aqueous solution at room temperature for 12 and 24 h.

be carried on in the future work. This novel anodic treatment in DES shows the feasibility of conversion film formation on Mg alloys.

The porous structures of the conversion films may not be a perfect choice for corrosion protections. However, effective enhancement in corrosion resistance can be obtained by further surface modifications [19]. Fig. 7 shows the wettability of the conversion films after superhyrophobic (SHS-25, SHS-50) and slippery (SLIPS-25 and SLIPS-50) modifications. It can be seen that superhydrophobic and slippery surfaces are achieved either for the CF-25 or for the CF-50. The water (4 μl) CA value of the SHS-50 (158 ± 1°) is a little larger than that of the SHS-25 (154 ± 1°) though their SA values are both very small (~1°). It is ascribed to the rougher surface of the CF-50 compared with the CF-25 (see Fig. 2e and f). After slippery modification, the two conversion films possess similar water CA values (about 117°). Water droplets (8 μl) slowly slide off the SLIPSs as the substrates are tilted by ~10°. A higher CA hysteresis is found for the SLIPS-25 (~13°) than that for the SLIPS-50 (~8°), which might be ascribed to the nonuniformity of the CF-25 (see Fig. 2b). Therefore, water droplets would be pinned on the surface [47].

Fig. 8 exhibits the polarization curves of the bare AZ31B, CF-25, CF-50, SHS-50 and SLIPS-50 performed in a 3.5 wt% NaCl aqueous solution at room temperature. The E_{corr} and i_{corr} are derived from the polarization curves and summarized in Table 1. In the polarization curves, the cathodic branch is attributed to hydrogen evolution, while the anodic branch shows important features related to the anodic behavior of the specimen. Significantly decreased anodic current densities are detected for the coated specimens (CF-25 and CF-50) compared with the bare substrate. It suggests that the corrosion resistance of the AZ31B Mg alloy is effectively enhanced by anodic treatment processes in the DES. As listed in Table 1, the CF-25 and CF-50 exhibit lower i_{corr} than the bare Mg alloy substrate although they possess almost the same E_{corr} as the substrate. Moreover, the higher anodic current density applied in the anodic treatment, the better corrosion resistance of the conversion film is obtained. Since the Mg alloy substrate has a significant influence on the corrosion resistance of the thin conversion film, it is reasonable to get the adjacent E_{corr} values of the AZ31B, CF-25 and CF-50. The i_{corr} of the conversion film is further decreased by 2 orders of magnitude after the SHS or SLIPS modification. The air pocket layer trapped in the grooves and self-assembled monolayers (SAMs) of PTES formed on the SHS-50 surface are responsible for the significant decrease of i_{corr} and positive shift of E_{corr}. Air pockets and SAMs serve as corrosion barriers to isolate the substrate or conversion film from NaCl solution, which leads to a small contact area of the solid/liquid interface. As a consequence, it makes the anodic branch look like a passivation plateau with low anodic current density between the potentials of −1.45 V and − 1.36 V. The abrupt rise of anodic current density at −1.36 V should be attributed to the collapse of SHS. Theoretically, no Faraday process occurs in a fully lubricant infused SLIPS and negligible current should be detected owing to the charging/discharging of the double layer capacitance [19,48]. However, the SLIPS-50 was vertically hung

for 3 days to drain off the excess lubricant in this work. The jagged arrays are very likely to be exposed without the protection of lubricant, which is apt to be corroded. Corrosion aggravates rapidly at these defects without passivation. Consequently, the E_{corr} of the SLIPS-50 is similar to that of the SHS-50, whereas the i_{corr} of the SLIPS-50 is detected though it is lower than that of the SHS-50. As an additional corrosion barrier, the infused lubricant layer further prevents the substrate from corrosion. It can be seen that the low anodic current density of SLIPS-50 maintains until SLIPS collapses at the potential of −1.31 V.

The immersion test was performed by exposing the bare AZ31B, CF-25, CF-50, SHS-50 and SLIPS-50 in the 3.5 wt% NaCl aqueous solution for 12 and 24 h. The optical photographs after immersion test are shown in Fig. 9. After 12 h of immersion, these specimens exhibited different levels of corrosion. An uneven gray film with some white pits was covered on the bare AZ31B indicating a severe corrosion of the substrate. It seemed that the as-prepared conversion films of the CF-25 and CF-50 were desquamated leaving another gray film without visible corrosion pits. The partial desquamation of the CF-50 suggests a mitigation of corrosion compared to the CF-25, which is in accordance with the polarization curves. Accordingly, a localized area was corroded for the SHS-50 with enhanced corrosion resistance and no visible corrosion trace was observed for the SLIPS-50. Only a small corrosion pit was found on the SLIPS-50 after 24 h of immersion, which originated from the desquamated region undergoing 12 h of immersion. During the immersion, corrosion aggravated at the defects of the desquamated regions for the other specimens. It can be speculated that the conversion films in the immersion test should involve the following corrosion processes. Firstly, aggressive Cl^- in the solution attacks and destroys the exposed $MgCO_3$ based conversion film, which results in a dissolution/desquamation of the conversion film. Then the inner Mg alloy substrate is corroded to form gray conversion films. Finally, some defects in the film regions are further corroded by Cl^- leaving white corrosion pits on the surface. The enhanced corrosion resistance of the SHS and SLIPS might be attributed to the less contact area between the conversion films and corrosive solution supported by trapped air and infused lubricant in the films.

4. Conclusions

The anodic treatment was carried out in the DES for preparing conversion films on Mg alloys. The as-prepared conversion film showed a rough surface with interconnected porous networks or jagged nanorod arrays depending on the applied anodic current density. XRD results indicated that the surface crystallographic orientation of the Mg alloy was changed after the anodic treatment. TEM and XPS analyses confirmed the formation of $MgCO_3$ and little MgO in the conversion film. The underlying mechanism for the conversion film growth was proposed, which might involve the DES decomposition at the anodic voltage and the interaction between the substrate and DES-derived species. Superhydrophobic and slippery surfaces were further achieved on the CF-25 and CF-50 by surface modifications. The i_{corr} of the Mg alloy with conversion films was decreased to 66.5 (CF-25) and 27.7 (CF-50) μA cm^{-2} from 988 μA cm^{-2} of the bare substrate. Moreover, the i_{corr} was further decreased by 2 orders of magnitude after the superhydrophobic or slippery modifications, indicating a significant enhancement in corrosion resistance. Passivation plateaus were found in the polarization curves for the SHS-50 and SLIPS-50.

Acknowledgments

This work was supported by the State Key Laboratory for Mechanical Behavior of Materials.

References

[1] Q.H. Yuan, X.S. Zeng, Y. Liu, L. Luo, J.B. Wu, Y.C. Wang, G.H. Zhou, Carbon 96 (2016) 843–855.
[2] L. Mao, L. Shen, J.H. Chen, Y. Wu, M. Kwak, Y. Lu, Q. Xue, J. Pei, L. Zhang, G.Y. Yuan, R. Fan, J.B. Ge, W.J. Ding, ACS Appl. Mater. Interfaces 7 (2015) 5320–5330.
[3] G.S. Frankel, Nat. Mater. 14 (2015) 1189–1190.
[4] W.Q. Xu, N. Birbilis, G. Sha, Y. Wang, J.E. Daniels, Y. Xiao, M. Ferry, Nat. Mater. 14 (2015) 1229–1235.
[5] F.Y. Cao, G.L. Song, A. Atrens, Corros. Sci. 111 (2016) 835–845.
[6] S. Heise, S. Virtanen, A.R. Boccaccini, J. Biomed. Mater. Res., Part A 104 (2016) 2628–2641.
[7] S. Pommiers, J. Frayret, A. Castetbon, M. Potin-Gautier, Corros. Sci. 84 (2014) 135–146.
[8] G.S. Wu, J.M. Ibrahim, P.K. Chu, Surf. Coat. Technol. 233 (2013) 2–12.
[9] L.A. Hernández-Alvarado, L.S. Hernández, M.A. Lomelí, J.M. Miranda, L. Narváez, I. Diaz, M.L. Escudero, J. Alloys Compd. 664 (2016) 609–618.
[10] S. Pommiers-Belin, J. Frayret, A. Uhart, J.B. Ledeuil, J.C. Dupin, A. Castetbon, M. Potin-Gautier, Appl. Surf. Sci. 298 (2014) 199–207.
[11] J. Jayaraj, S. Amruth Raj, A. Srinivasan, S. Ananthakumar, U.T.S. Pillai, N.G.K. Dhaipule, U.K. Mudali, Corros. Sci. 113 (2016) 104–115.
[12] R.C. Zeng, F. Zhang, Z.D. Lan, H.Z. Cui, E.H. Han, Corros. Sci. 88 (2014) 452–459.
[13] L.Y. Niu, Z.H. Jiang, G.Y. Li, C.D. Gu, J.S. Lian, Surf. Coat. Technol. 200 (2006) 3021–3026.
[14] X.L. Liu, T. Zhang, Y.W. Shao, G.Z. Meng, F.H. Wang, Corros. Sci. 51 (2009) 2685–2693.
[15] H.H. Elsentriecy, K. Azumi, H. Konno, Electrochim. Acta 53 (2008) 4267–4275.
[16] K. Li, J.Y. Liu, T. Lei, T. Xiao, Appl. Surf. Sci. 353 (2015) 811–819.
[17] L.Y. Niu, S.H. Chang, X. Tong, G.Y. Li, Z.M. Shi, J. Alloys Compd. 617 (2014) 214–218.
[18] S.Y. Jian, Y.R. Chu, C.S. Lin, Corros. Sci. 93 (2015) 301–309.
[19] J.L. Zhang, C.D. Gu, J.P. Tu, ACS Appl. Mater. Interfaces 9 (2017) 11247–11257.
[20] N. Kamiyama, G. Panomsuwan, E. Yamamoto, T. Sudare, N. Saito, T. Ishizaki, Surf. Coat. Technol. 286 (2016) 172–177.
[21] R.C. Zeng, Z.G. Liu, F. Zhang, S.Q. Li, H.Z. Cui, E.H. Han, J. Mater. Chem. A 2 (2014) 13049–13057.
[22] Y.C. Wang, J.Y. Lin, C.H. Wang, P.L. Huang, S.L. Lee, J.K. Chang, RSC Adv. 4 (2014) 35298–35301.
[23] C.D. Gu, W. Yan, J.L. Zhang, J.P. Tu, Corros. Sci. 106 (2016) 108–116.
[24] Y.F. Zhang, X. Liu, S.S. Jamali, B.R.W. Hinton, S.E. Moulton, G.G. Wallace, M. Forsyth, Surf. Coat. Technol. 296 (2016) 192–202.
[25] S.G. Zhang, Q.H. Zhang, Y. Zhang, Z.J. Chen, M. Watanabe, Y.Q. Deng, Prog. Mater. Sci. 77 (2016) 80–124.
[26] Y. Ma, F. Han, Z. Li, C.G. Xia, ACS Sustain. Chem. Eng. 4 (2016) 633–639.
[27] H.H. Elsentriecy, J. Qu, H.M. Luo, H.M. Meyer Iii, C. Ma, M.F. Chi, Thin Solid Films 568 (2014) 44–51.
[28] P.P. Huang, J.A. Latham, D.R. MacFarlane, P.C. Howlett, M. Forsyth, Electrochim. Acta 110 (2013) 501–510.
[29] J. Efthimiadis, W.C. Neil, A. Bunter, P.C. Howlett, B.R.W. Hinton, D.R. MacFarlane, M. Forsyth, ACS Appl. Mater. Interfaces 2 (2010) 1317–1323.
[30] A.P. Abbott, D. Boothby, G. Capper, D.L. Davies, R.K. Rasheed, J. Am. Chem. Soc. 126 (2004) 9142–9147.
[31] D.V. Wagle, H. Zhao, G.A. Baker, Acc. Chem. Res. 47 (2014) 2299–2308.
[32] E.L. Smith, A.P. Abbott, K.S. Ryder, Chem. Rev. 114 (2014) 11060–11082.
[33] X. Ge, C.D. Gu, Y. Lu, X.L. Wang, J.P. Tu, J. Mater. Chem. A 1 (2013) 13454–13461.
[34] J.L. Zhang, C.D. Gu, Y.Y. Tong, W. Yan, J.P. Tu, Adv. Mater. Interfaces 3 (2016) 1500694.
[35] K. Haerens, E. Matthijs, K. Binnemans, B. Van der Bruggen, Green Chem. 11 (2009) 1357–1365.
[36] A.P. Abbott, E.I. Ahmed, R.C. Harris, K.S. Ryder, Green Chem. 16 (2014) 4156–4161.
[37] A.P. Abbott, G. Capper, B.G. Swain, D.A. Wheeler, Trans. IMF 83 (2005) 51–53.
[38] J.L. Zhang, C.D. Gu, S. Fashu, Y.Y. Tong, M.L. Huang, X.L. Wang, J.P. Tu, J. Electrochem. Soc. 162 (2015) D1–D8.
[39] Y. Zheng, R.C. Peng, H.Y. Jin, Y.B. Luo, Y. Ping, Surf. Coat. Technol. 325 (2017) 539–547.
[40] S. Ardizzone, C.L. Bianchi, M. Fadoni, B. Vercelli, Appl. Surf. Sci. 119 (1997) 253–259.
[41] K.S. Zhang, S.B. Wu, X.L. Wang, J.Y. He, B. Sun, Y. Jia, T. Luo, F.L. Meng, Z. Jin, D.Y. Lin, W. Shen, L.T. Kong, J.H. Liu, J. Colloid Interface Sci. 446 (2015) 194–202.
[42] S. Frykstrand, J. Forsgren, A. Mihranyan, M. Strømme, Microporous Mesoporous Mater. 190 (2014) 99–104.
[43] Z.P. Zhang, Y.J. Zheng, J.X. Zhang, Q. Zhang, J.P. Chen, Z.M. Liu, X.M. Liang, Cryst. Growth Des. 7 (2007) 337–342.
[44] J. Bhatt, D. Mondal, K. Prasad, J. Cryst. Growth 442 (2016) 95–97.
[45] E. Kirinovic, A.R. Leichtfuss, C. Navizaga, H.Y. Zhang, J.D. Schuttlefield Christus, J. Baltrusaitis, ACS Sustain. Chem. Eng. 5 (2017) 1567–1577.
[46] Y.H. Wu, W.J. Zhao, W.R. Wang, W.J. Sui, RSC Adv. 6 (2016) 5100–5110.
[47] P. Kim, T.S. Wong, J. Alvarenga, M.J. Kreder, W.E. Adorno-Martinez, J. Aizenberg, ACS Nano 6 (2012) 6569–6577.
[48] R. Qiu, Q. Zhang, P. Wang, L.N. Jiang, J. Hou, W.M. Guo, H.X. Zhang, Colloids Surf. A Physicochem. Eng. Asp. 453 (2014) 132–141.